13th World Conference on Earthquake Engineering
Vancouver, B.C., Canada
August 1-6, 2004
Paper No. 279

STRENGTH AND DEFORMATION CAPACITY OF REINFORCED CONCRETE COLUMNS WITH LIMITED DUCTILITY

Halil SEZEN[1], and Jack P. MOEHLE[2]

SUMMARY

This paper presents the results from an experimental and analytical research program investigating the axial and lateral behavior of reinforced concrete columns with poorly detailed transverse reinforcement. As part of the experimental research, four full-scale reinforced concrete building columns were tested under constant and varying axial loads and cyclic lateral loads. The columns, with nominally identical properties, had details typical of those found in low seismic regions or those permitted in high seismic regions in the U.S. until mid-1970s. The test columns were designed to experience significant stiffness and strength degradation due to shear failure after flexural yielding. Column deformations due to flexure, longitudinal bar slip at column supports, and shear are investigated. Flexure deformations are computed from fiber section moment-curvature analysis with uniaxial material properties. A bar-slip model using moment-curvature analysis results is developed to predict deformations due to longitudinal bar slip at beam-column interfaces. A shear strength model is proposed to predict the column shear strength considering the effects of key variables such as axial load, column aspect ratio, transverse reinforcement, and displacement ductility demand.

INTRODUCTION

Structural collapse under combined action of seismic and gravity loads is a limit state of great interest in design of new reinforced concrete buildings and evaluation of existing buildings. Seismic evaluation and rehabilitation guidelines such as FEMA 356 [1] identify shear and gravity load failure of columns as the critical failure mode associated with structural instability or collapse. Usually these failures occur in a brittle manner at relatively small lateral drifts. Many examples of such column failures were observed and documented during recent earthquakes (Figure 1). Most commonly, these columns include insufficient transverse reinforcement, involving both wide spacing and inadequate anchorage with 90-degree end hooks.

[1] Assistant Professor, The Ohio State University, Columbus, Ohio, USA. E-mail: sezen.1@osu.edu
[2] Professor, Pacific Earthquake Engineering Research Center, University of California, Berkeley, USA. E-mail: moehle@peer.berkeley.edu

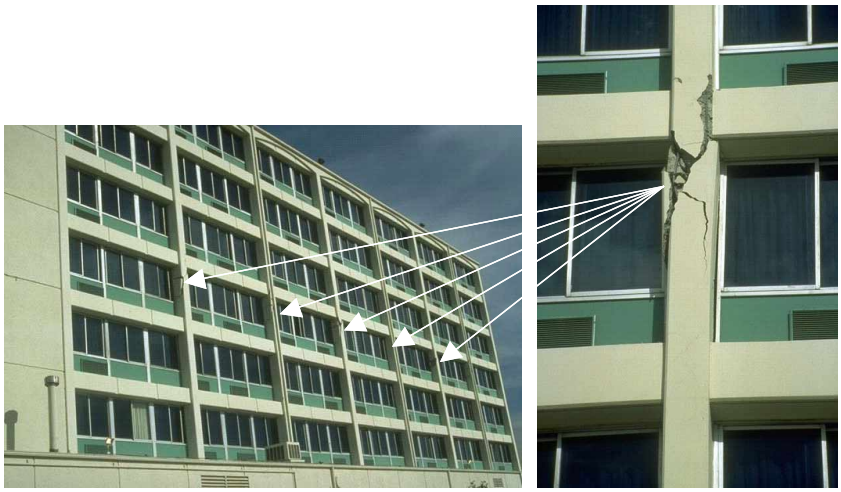

Figure 1 Column failures in a hotel building in the 1994 Northridge, California earthquake

This research program was initiated to examine the shear and gravity load failure of reinforced concrete columns with limited strength and deformation capacity. As part of the experimental research, four full-scale columns with nominally identical properties and details were tested. This paper presents some of the test results as well as analytical models to predict the deformation response and shear strength of lightly reinforced columns.

EXPERIMENTAL INVESTIGATION

Test program

Four columns were designed and tested in double curvature quasi-statically. The columns had cross-sections of 457 mm by 457 mm, and were approximately 2950 mm tall. The test specimen elevation, typical column cross-section, and test setup are shown in Figure 2. The column design details, geometry, and material properties are representative of those of older columns in existing buildings, and are based on the studies of older building code requirements and similar columns tested previously [2]. Detailed

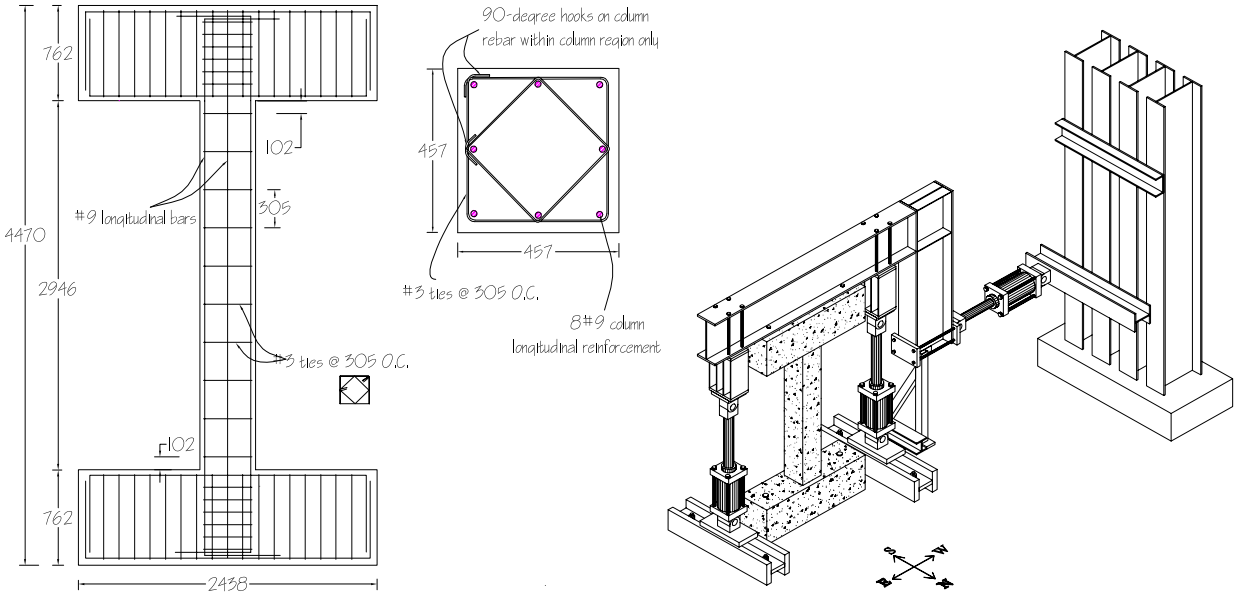

Figure 2 Specimen elevation, cross-section details, and test setup (units in mm)

description of test specimens, construction process, test setup, loading conditions, and test results are reported by [3].

The specimens included 760 mm deep, 2440 mm long, heavily reinforced top and bottom beams, which simulated a rigid foundation or a rigid floor slab. The specimens were loaded axially using two 1780-kN-capacity vertical hydraulic actuators while maintaining zero rotation of the top beam. Uni-directional lateral load was applied by a displacement controlled 2220-kN-capacity horizontal hydraulic actuator. The average measured concrete cylinder strength was about 21 MPa on the day of tests. Eight 28.7-mm-diameter longitudinal bars were used for a longitudinal reinforcement ratio of 2.5 percent. The average yield strength and ultimate strength of the longitudinal bars were 438 MPa and 645 MPa, respectively. The measured yield strength and ultimate strength of 9.5-mm-diameter deformed transverse reinforcement were 476 MPa and 724 MPa, respectively.

The first three specimens were subjected to the same lateral displacement history, which included application of three cycles of fraction of nominal yield displacement, Δ_y initially. Then, the magnitude of displacement cycles was increased incrementally, i.e., three cycles of Δ_y, $2\Delta_y$, $3\Delta_y$, etc., until the specimen failed. The last specimen was loaded monotonically to failure after the yield displacement was reached. The first and last test columns, Specimen-1 and Specimen-4, were subjected to constant compressive axial load of 667 kN. Specimen-2 was subjected to a constant axial load of 2670 kN. These three columns with constant axial load were intended to represent columns in a gravity load carrying frame system. As shown in Figure 3, the axial loads 667 kN and 2670 kN correspond nominally to the same flexural strength on the axial load-moment interaction diagram. Therefore, the three columns subjected to constant axial loads had the same theoretical shear demand. Specimen-3, which represents of a corner column or an end column of a building frame, was subjected to varying axial load. The axial load on this column was a linear function of lateral load, and varied between 2670 kN in compression and 250 kN in tension.

Strain gages were attached on the longitudinal and transverse reinforcement to monitor the strain variations along the height of the columns. Figure 4a shows the arrangement of strain gages attached on the steel bars. Local deformations were measured over the height of test columns using linear displacement potentiometers. Figure 4b shows the arrangement of displacement potentiometers installed on both sides of the column. Global deformations between fixed points in the laboratory and various points on the specimen were also monitored during the tests (Figure 4c). Instruments including

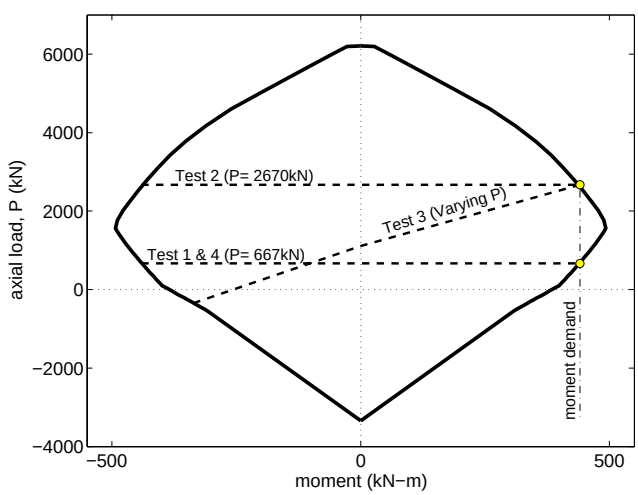

Figure 3 Arrangement of displacement potentiometers and strain gages

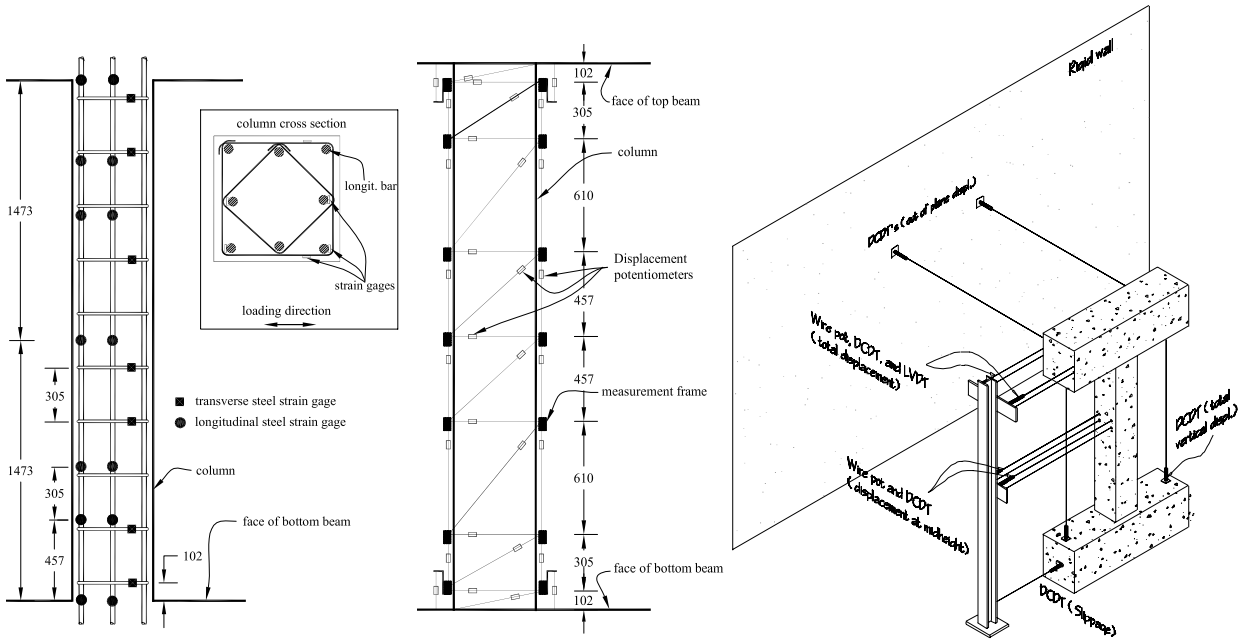

(a) **(b)** **(c)**

Figure 4 Instrumentation to measure: a) longitudinal and transverse steel strains, b) local deformations, and c) global deformations

linear variable differential transducers (LVDTs), direct current differential transducers (DCDTs) and wire potentiometers were used to measure the global deformations such as total column lateral and vertical displacements.

Description of column behavior

Figure 5 shows the damage and crack distribution on each face of the specimens after the completion of yield displacement cycles and at failure. Figure 6 shows the measured lateral load versus lateral displacements for all columns. Before the tests, horizontal hairline cracks apparently due to shrinkage were uniformly distributed over the height of the columns. During the initial cycles up to yield displacement, all columns behaved similarly, and had some inclined cracks near the top and bottom ends (Figure 5a).

Specimen-1 lost its lateral strength substantially during the displacement cycles of two times yield displacement (56 mm). At larger displacements, the column sustained significant damage including large diagonal cracks and concrete spalling. However, it was able to carry the applied axial load until the end of the test where no lateral load carrying capacity was left. The lateral strength and stiffness of Specimen-2, which was subjected to very high axial load, were noticeably higher during low displacement cycles. However, the specimen had a sudden axial and shear failure at relatively low displacement. Final failure occurred shortly after an apparent longitudinal reinforcement bond failure over the length of the column. No diagonal cracks were observed around the midheight of the column, and longitudinal bars did not reach their yield strength before failure occurred. Specimen-3 with varying axial load had larger lateral strength and stiffness when subjected to larger compressive axial loads (Figure 6). Under tensile or low compressive axial loads, the strength degradation was less significant (Figure 6). Under monotonic lateral load, the lateral displacement capacity of Specimen-4 increased as compared with the displacement capacity under cyclic loading (Specimen-1). In addition, the reduction in the lateral strength was slower, apparently because degradation in resistance mechanisms was less severe under monotonic loading.

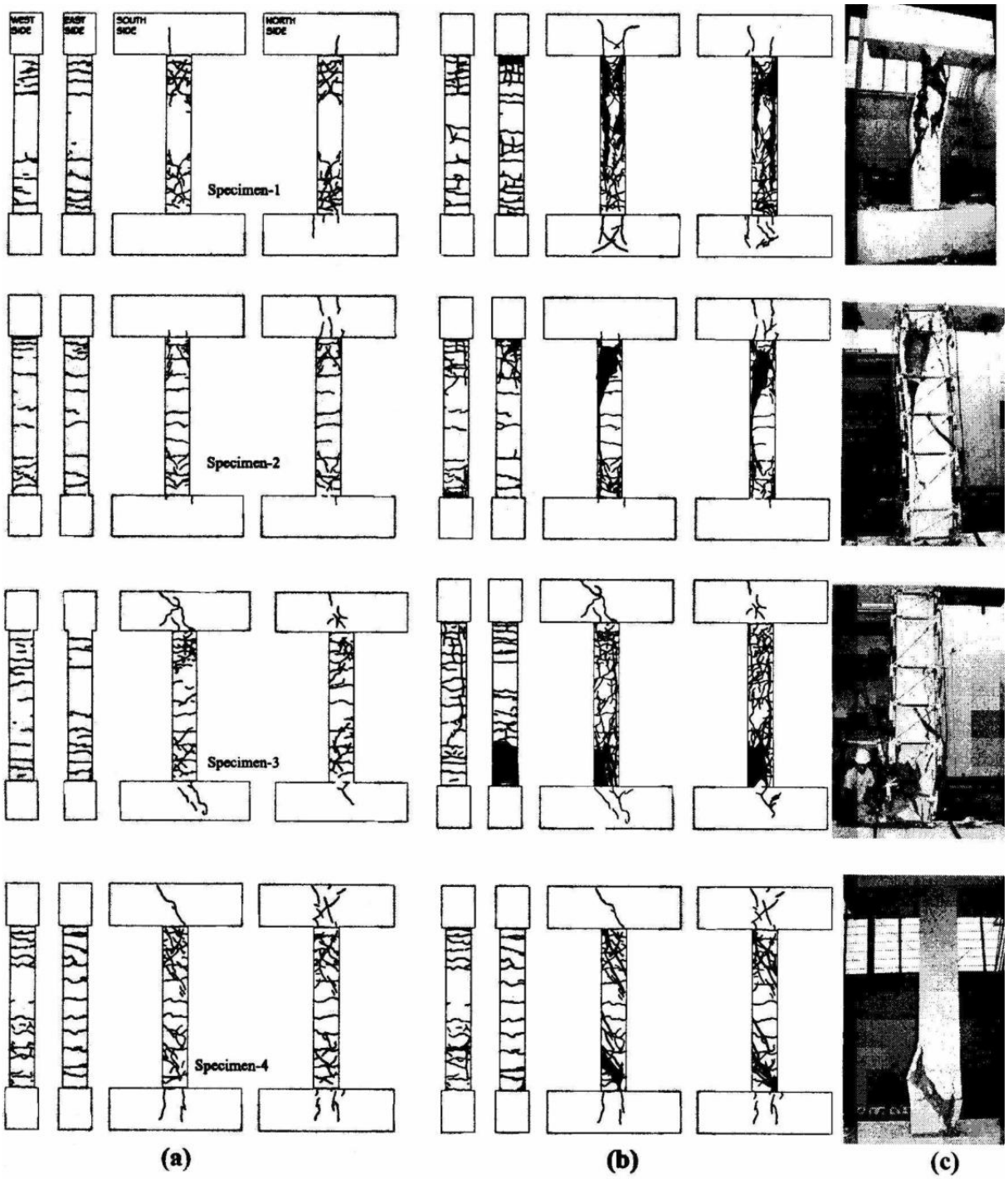

Figure 5 Crack pattern at: a) yield displacement, b) at failure; and c) damage at failure

The measured relations between the vertical displacements and lateral load shown in Figure 6 indicate that initially vertical displacements were directly related to magnitude of applied axial load. This is primarily because columns tend to elongate with increasing lateral deformation as a result of crack opening along the column height. As the columns further damaged, the tendency to elongate reverses, and continued shortening progresses mainly through sliding along diagonal cracks.

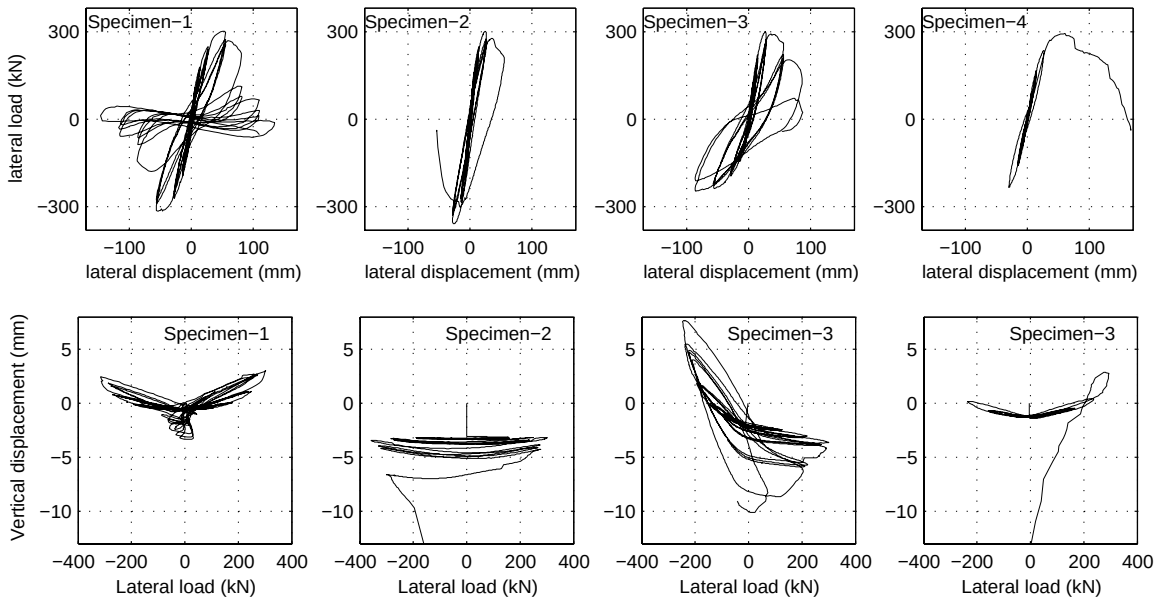

Figure 6 Lateral load-displacement, and vertical displacement-lateral load relations

EVALUATION OF TEST RESULTS AND ANALYTICAL WORK

Local vertical displacements, measured by the displacement potentiometers installed on each side of the columns (Figure 4a) were used to compute average curvatures over the column height. Average curvature profiles for each column are shown in Figure 7. Curvature profiles are shown at three lateral displacement levels in both loading directions. Apparently, because of additional deformations due to longitudinal bar slip, the measured average curvatures were much larger near the beam-column interfaces at the top and bottom of columns. Except for these large curvatures near the top and bottom, in general, the average

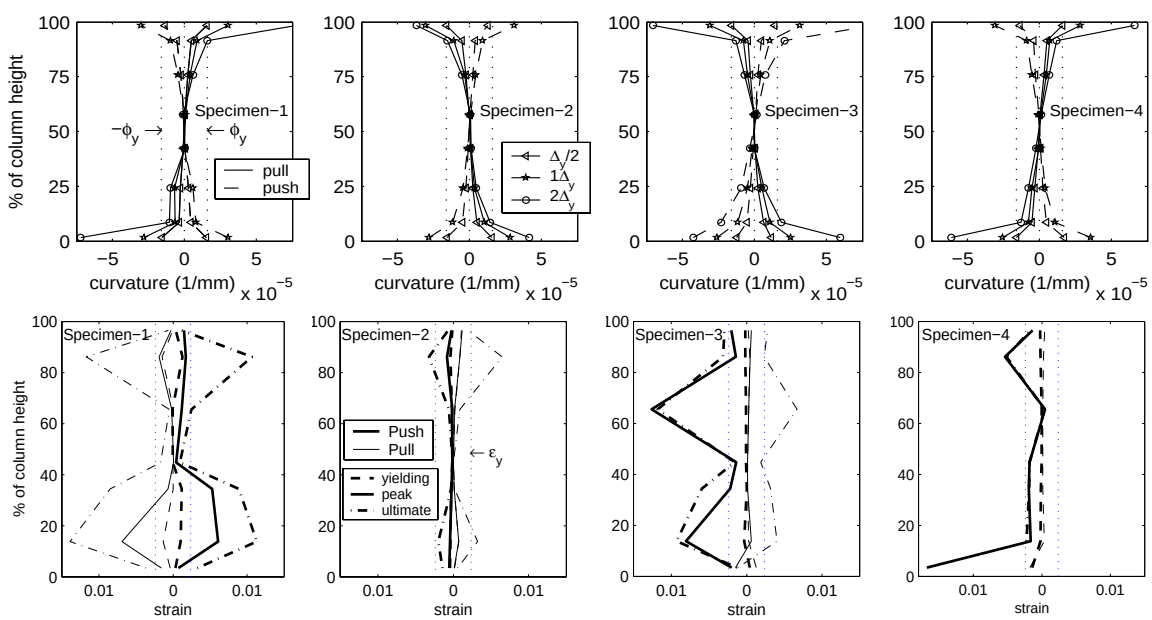

Figure 7 Average measured curvature profiles (top row), and measured transverse steel strain distributions over the height of columns (bottom row)

curvatures varied almost linearly over the height and were smaller than the calculated yield curvature, ϕ_y. Also shown in Figure 7 are the transverse reinforcement strain distributions over the height of columns. The strains were plotted in each loading direction at first yielding in the longitudinal bars, at peak lateral load, and at loss of lateral capacity (ultimate), which is assumed to occur when the lateral load drops to 80 percent of peak lateral strength is reached. At peak and ultimate levels, the transverse reinforcement strains tend to be the largest some short distance away from column ends, where most of the damage and extensive cracking were observed due to combined high flexural and shear demand. As the damage progresses, more cracks intersect the transverse reinforcement and consequently increase the strains in the bars crossing the cracks. For instance, in Specimen-2 with less damage and less number of cracks at the onset of failure, the strains in the transverse direction were much smaller prior to failure.

Deformation components

As illustrated in Figure 8, total column lateral displacement measured at the top of each column can be assumed to be the summation of deformations due to: a) flexure, $\Delta_{flexure}$; b) longitudinal bar slip at column ends, Δ_{slip}; and c) shear, Δ_{shear}. Experimental flexure, bar slip, and shear deformations are obtained and

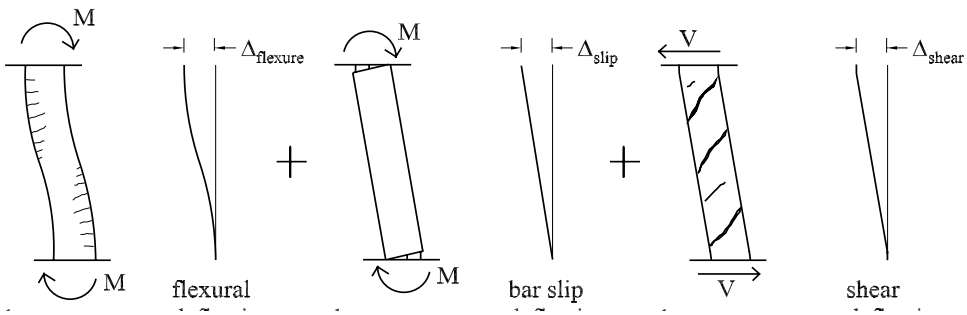

Figure 8 Contribution of displacement components to total lateral displacement

presented in the following sections. Figure 9 shows the contribution of these deformation components to the total column lateral displacement at peak displacement during each displacement cycle. The results indicate that approximately 40 to 60 percent of total lateral displacement is due to flexure, while 25 to 40 percent is due to bar slip deformations. Typically the shear displacement component is relatively small especially in the elastic range and under very high axial loads. However, the contribution of shear deformations can increase significantly as in Specimen-1. In this column, the contribution of shear deformations grew gradually to about 20 percent of the total deformation at a displacement ductility of two, at which time shear strength degradation became severe and shear deformations increased dramatically to about 40 percent of total displacement.

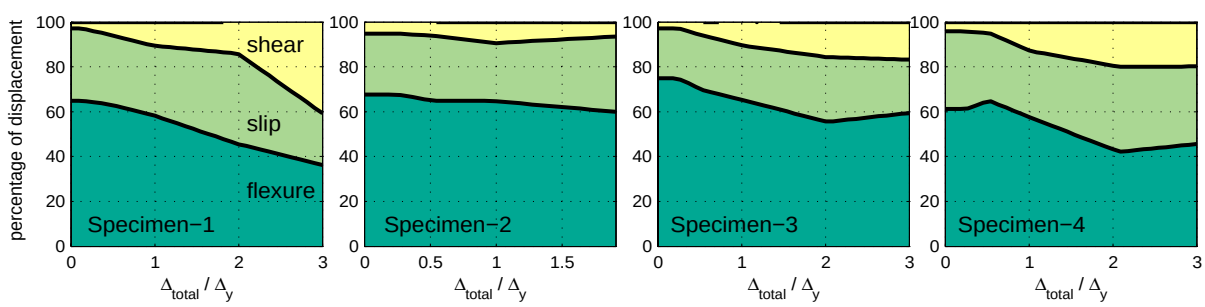

Figure 9 Contribution of displacement components to total lateral displacement

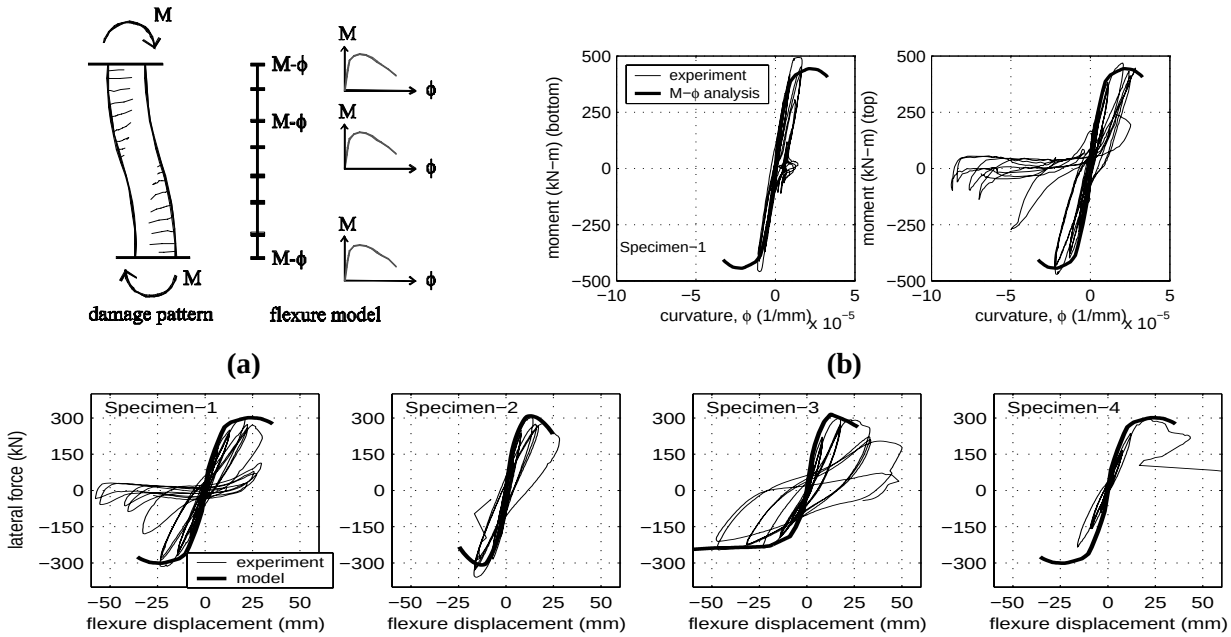

Figure 10 a) Curvatures at the top and bottom of Specimen-1, b) flexure model, and c) lateral load-flexural displacement relations

Flexure response

For a typical beam-column frame member, lateral displacement due to flexure can be calculated by integrating the flexural curvatures, ϕ along the height of the member: $\Delta_{flexure} = \int_0^l \phi\, x\, dx$ (Figure 10a). As an example, Figure 10b shows the cyclic lateral load-flexural curvature relations measured at the top and bottom beam-column interfaces of Specimen-1. The curvatures at these cross-sections do not include the effect of longitudinal bar slip deformations. In order to eliminate the effect of bar slip deformations on the measured total curvatures at column ends (Figure 7), the flexural curvatures are assumed to vary linearly near the column supports. Figure 10c shows the moment-flexural displacement relations for the columns, which were computed by integrating the sectional curvatures over the column height as illustrated in Figure 10a. Calculated monotonic section moment-curvature relations at the top and bottom beam-column interface of Specimen-1 (Figure 10b), and the corresponding calculated monotonic lateral load-flexure displacement relations for all columns (Figure 10c) are also plotted. The monotonic moment-curvature relation is computed using the test column cross section discretized into multiple fibers with uniaxial material properties [4]. The uniaxial stress-strain model for the longitudinal reinforcing bars was based on measured stress-strain relations from steel coupon tests. A combination of confined and unconfined concrete models was used to represent the concrete behavior (Figure 11). Previous research [5] suggests that the concrete compressive strength increases if sufficient transverse reinforcement is provided. In this research, the nonlinear concrete stress-strain relation between the zero and peak concrete strength is modeled using the procedure developed by Mander et al. [5]. Figure 11 shows that, for strains smaller than 0.002, the confined concrete model compares very well with the measured stress-strain relations from concrete cylinder tests. Beyond the peak confined stress, the concrete is assumed to unload more rapidly than suggested by the Mander et al. model because, in this study, the transverse reinforcement spacing is relatively large and is unable to restrain the cracked concrete core. For the post-peak behavior, the unconfined concrete model with a descending straight-line stress-strain relationship developed by Roy and Sozen [6] was used.

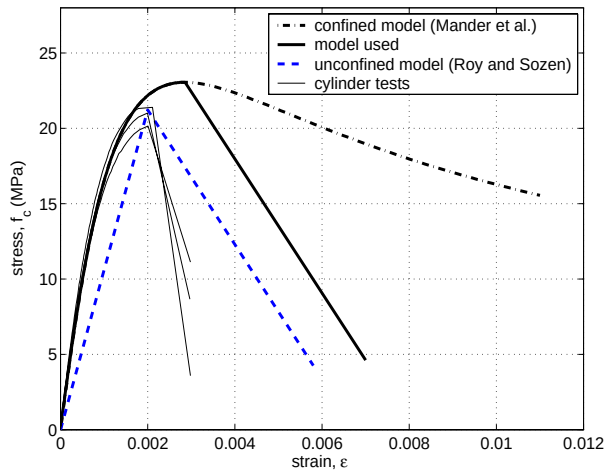

Figure 11 Compressive stress-strain relations for concrete

Bar slip deformations

Elongation and slip of the tensile reinforcement at beam-column interfaces could result in significant fixed-end rotations that are not included in the flexural analysis. These additional rotations at beam-column fixed-ends can increase the total member lateral displacement significantly. Figure 9 indicates that up to 40 percent of total lateral displacement can be due to longitudinal bar slip.

The relation between the cross-sectional moment and strain in the tensile reinforcement can be computed as part of the moment-curvature analysis. The calculated section moment-longitudinal bar strain relations are compared with the measured cyclic moment-strain relations at the top and bottom of Specimen-1 (Figure 12). Figure 12 shows that, in the elastic range and during the first yield cycle, strains can be estimated reasonably well from the moment-curvature analysis.

As a result of bond deterioration between steel and concrete, and penetration and accumulation of axial strains along the tensile reinforcement inside the joint, the extension and slip of the reinforcing bar at the interface can be significant. The slip resulting from accumulated axial strains in the bar embedded in the joint can be calculated by integrating the strains over the portion of the bar between the interface and the point with no axial strain. Using a bilinear strain distribution shown in Figure 13, the slip can be determined from the following equation.

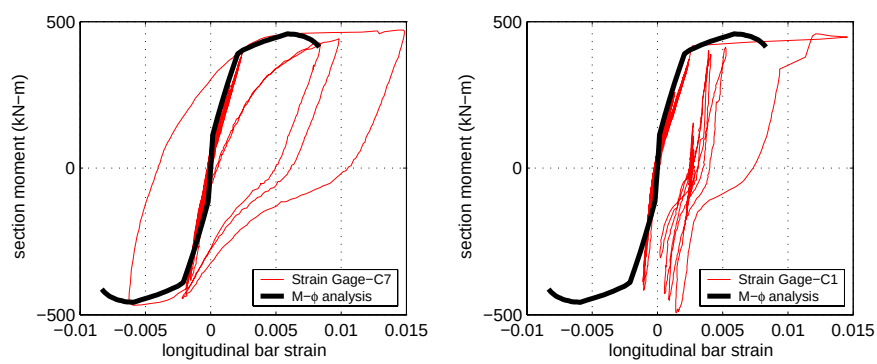

Figure 12 Calculated and measured strains at the top (Strain Gage-C7) and bottom (Strain Gage-C1) of Specimen-1

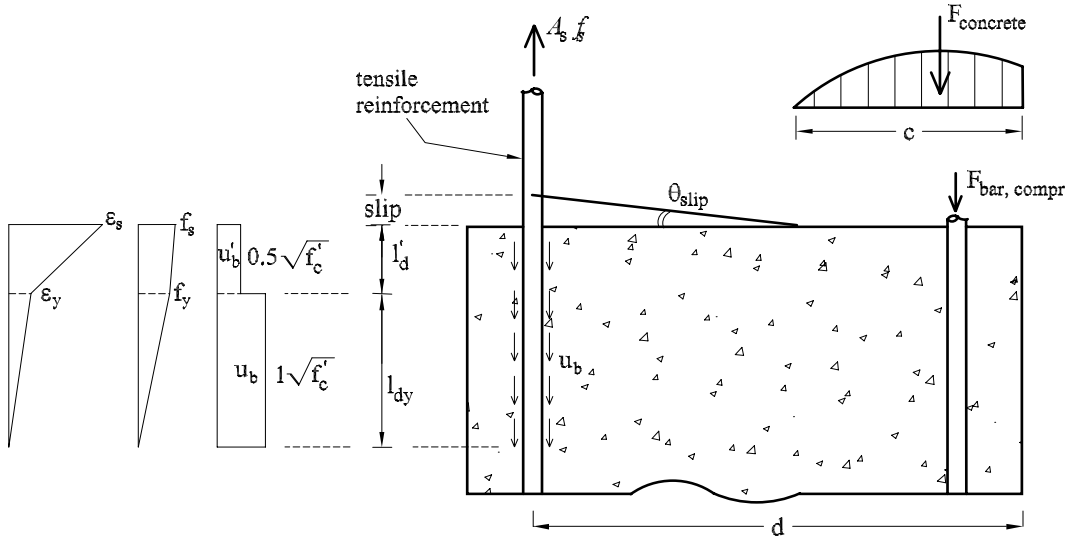

Figure 13 Illustration of bar slip deformation and forces at the beam-column interface

$$slip = \int_0^{l_d} \varepsilon \, dx = \frac{\varepsilon_s l_d}{2} \qquad \varepsilon_s \le \varepsilon_y$$
$$slip = \int_0^{l_{dy}} \varepsilon \, dx + \int_{l_{dy}}^{l_{dy}+l'_d} \varepsilon \, dx = \frac{\varepsilon_y l_{dy}}{2} + \frac{l'_d}{2}(\varepsilon_s + \varepsilon_y) \qquad \varepsilon_s > \varepsilon_y \tag{1}$$

where, *slip* = amount of reinforcing bar slip at beam-column interface, l_d = elastic development length, l'_d = development length over the inelastic portion of the bar, l_{dy} = development length corresponding to reinforcing bar yielding at interface, ε_s = strain in reinforcing bar, and ε_y = yield strain.

The development lengths over the elastic and inelastic portions of the bar can be calculated based on the equilibrium of forces in the bar at the interface, and the assumption of bi-uniform bond stress distribution, u_b [3]: $l_d = f_s d_b/(4u_b)$, $l_d' = (f_s - f_y) d_b/(4u'_b)$, where u_b = elastic uniform bond stress, u'_b = inelastic uniform bond stress, f_s = stress in reinforcing bar, f_y = steel yield stress, and d_b = bar diameter. Using equilibrium at first yielding in the longitudinal bar and assuming a linear strain distribution along the bar, by inserting $l_d = f_s d_b/(4u_b)$ into Equation 1, the average uniform bond stress at yielding, u_{by} can be calculated as a function of *slip*: $u_{by} = f_y^2 d_b/(8E_s slip)$. The slip was measured at the ends of twelve column specimens tested by [2] and [3]. Using the measured slip values at yield displacement, uniform bond stresses, u_{by} are calculated. The calculated bond stresses are normalized by $\sqrt{f'_c}$ and presented in Figure 14. For the twelve columns considered, the average bond stress is $0.95\sqrt{f'_c}$ MPa with a standard deviation of $0.2\sqrt{f'_c}$ MPa. In this study, a uniform bond stress, u_b of $1.0\sqrt{f'_c}$ MPa ($12\sqrt{f'_c}$ psi) is assumed in the elastic range (Figure 13). In the portion of the reinforcing bar over which the yield strain is exceeded, a uniform bond stress, u'_b of $0.5\sqrt{f'_c}$ MPa ($6\sqrt{f'_c}$ psi) is used as suggested by [7].

Figure 13 illustrates that the section rotation due to bar slip, θ_{slip} can be calculated by dividing the *slip* by the width of the open crack, which is the difference between the section depth, *d* and the neutral axis depth, *c*: $\theta_{slip} = slip/(d-c)$. This is based on the assumption that the section rotates about its neutral axis. Then, substitution of elastic and inelastic development lengths, l_d and l_d' into Equation 1 yields

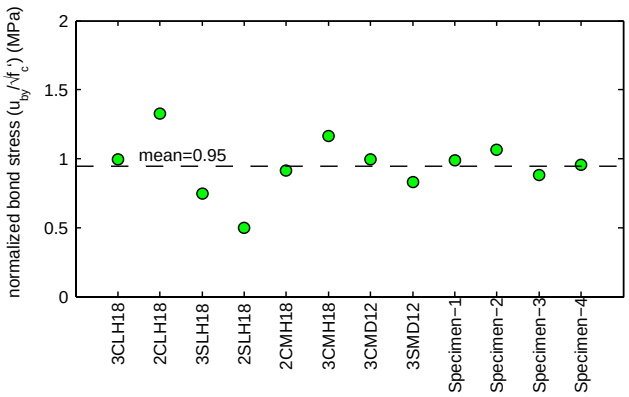

Figure 14 Calculated bond stresses at yield level

$$\theta_{slip} = \frac{\varepsilon_s f_s d_b}{8\sqrt{f_c'}(d-c)} \qquad \varepsilon_s \le \varepsilon_y$$

$$\theta_{slip} = \frac{d_b}{8\sqrt{f_c'}(d-c)}\left[\varepsilon_y f_y + 2(\varepsilon_s + \varepsilon_y)(f_s - f_y)\right] \qquad \varepsilon_s > \varepsilon_y \tag{2}$$

As shown in Figure 15a, the rotation due to bar slip, can be assumed to be concentrated at the beam-column interface in the form of rigid body rotation. If the slip rotation at the top and bottom of a double-curvature column with a length L is known, total lateral displacement due to bar slip can be calculated from

$$\Delta_{slip} = \left(\theta_{slip,top} + \theta_{slip,bottom}\right)L \tag{3}$$

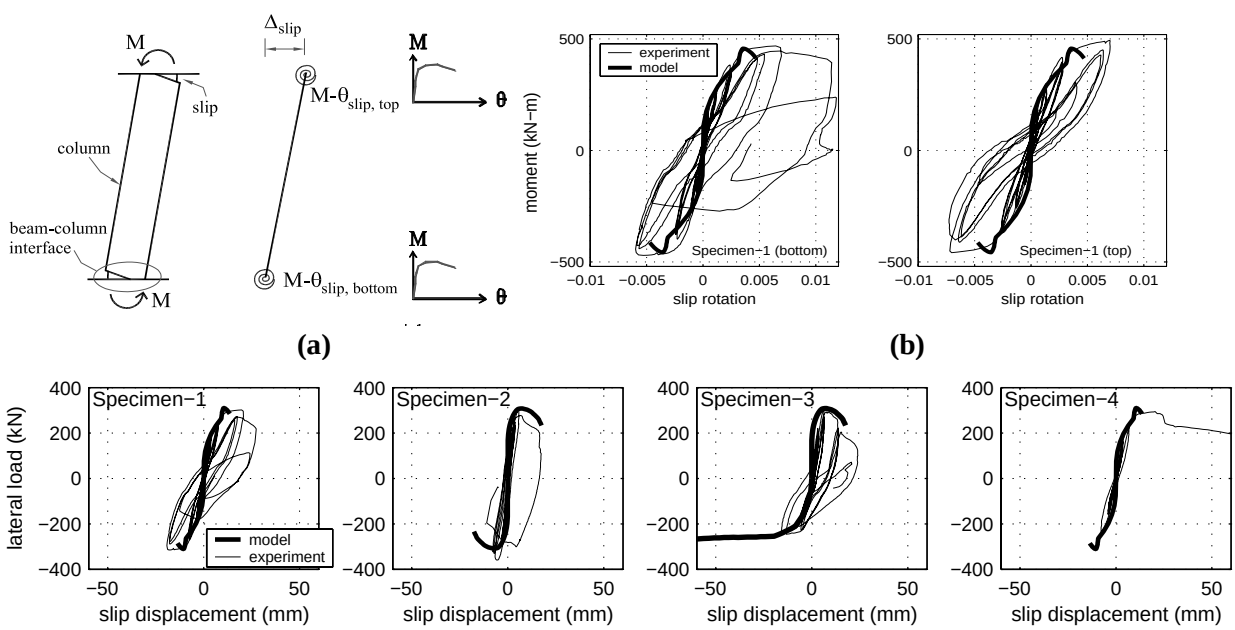

Figure 15 a) Slip displacement model, b) slip rotations at the top and bottom of Specimen-1, and c) lateral load-bar slip displacement relations

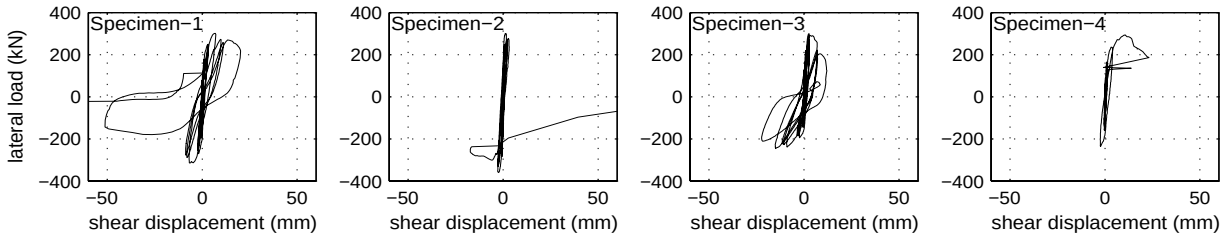

Figure 16 Measured lateral load-shear displacement relations

Using the longitudinal bar stress-strain relations calculated from fiber section moment-curvature analysis, (e.g., Figure 12), the section moment-slip rotation (Figure 15b) and column lateral load-slip displacement relations (Figure 15c) can be computed from Equations 2 and 3. The calculated and measured lateral load-slip displacement relations compare relatively well for the four column specimens tested in this study.

Shear deformations and shear strength

Local shear deformations along the height of the column and total shear displacement (Δ_{shear} in Figure 8) can be computed from the local deformation measurements (Figure 4a) using the principle of virtual work [3]. In this research it was observed that, in general, the shear deformations tend to increase within the upper and lower one third of the columns. This is consistent with the strains measured in the transverse reinforcement (Figure 7) and can be attributed to opening and closing of flexural and inclined cracks in those regions (see crack patterns in Figure 5). The measured lateral load-shear displacement relations for each test column are shown in Figure 16. Typically the shear displacements are relatively small before the development of large inclined cracks in the columns. For example, in Specimen-1, the sudden increase in the shear displacements in the first and second cycles of $3\Delta_y$ displacement level coincides with the extensive damage including development of large diagonal cracks during those cycles.

The columns tested in this study developed their flexural strength before shear failure followed by axial failure under low axial load, or shear failure combined with axial failure under very high axial load. Both Specimen-1 and Specimen-4 had shear and axial failures at a displacement ductility of approximately 3 and 6, respectively. Specimen-2, which was subjected to very high axial load, had combined shear and axial load failure at a displacement ductility of 2. One of the main objectives of this research was to investigate the vulnerability of lightly reinforced columns to shear failure including axial load effects. For this purpose, Sezen and Moehle [8] collected and analyzed experimental data from 51 test columns representative of columns that sustained shear failure following flexural yielding. For the test data considered, the variation of measured normalized shear strength as a function of key variables is plotted in Figure 17, where P = axial compressive load at the time of shear failure, a = distance from point of maximum moment to point of zero moment, d = distance from extreme compression fiber to centroid of

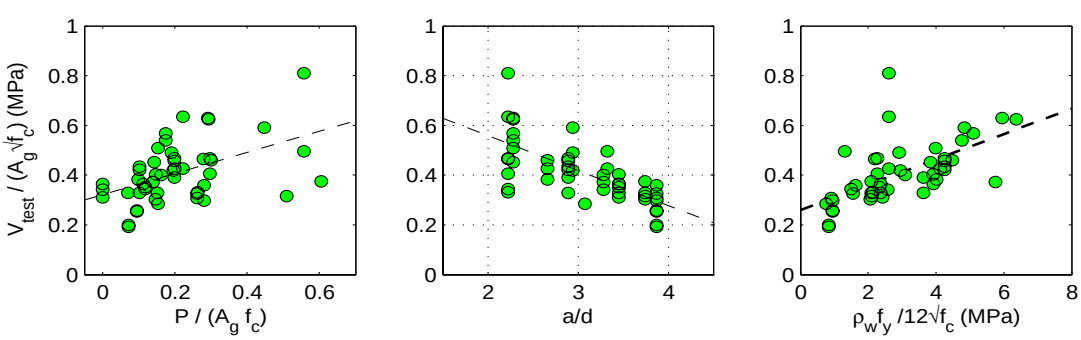

Figure 17 Effect of key variables on shear strength

longitudinal tension reinforcement, ρ_w = transverse reinforcement ratio = A_v/bs, A_v = cross-sectional area of transverse reinforcement parallel to the applied shear and having longitudinal spacing, s, and b = column width. The trends in the plotted data suggests that: a) shear strength increases with increasing compressive axial load; b) shear strength decreases with increasing aspect ratio, a/d; and c) shear strength increases with increasing amounts of transverse reinforcement.

Some researchers [9, 10] have proposed shear strength models in which concrete contribution to shear strength reduces with increasing displacement ductility demand. Others, such as [11], have found that column shear strength was independent of displacement ductility demand. Based on observations from column tests in this study, it was noted that with increasing displacement ductility, both the concrete and the reinforcement (hooks opening) and the interaction between concrete and reinforcement (bond-splitting cracks) contributed to progression of strength degradation. Thus, a strength degradation factor is applied to both concrete and reinforcement contributions to the shear strength ([2] and [8]). The shear strength model is expressed by the following equations:

$$V_n = V_c + V_s \tag{4}$$

$$V_s = k\frac{A_v f_y d}{s} \tag{5}$$

$$V_c = k\left(\frac{0.5\sqrt{f_c'}}{a/d}\sqrt{\frac{P}{0.5\sqrt{f_c'}A_g}}\right)0.8A_g \quad \text{(MPa)} \tag{6}$$

where V_n = nominal shear strength, V_c = nominal concrete contribution to shear strength, V_s = nominal transverse reinforcement contribution to shear strength, and k = a ductility related factor to account for effects of inelastic displacement cycles on shear strength degradation. Figure 18 plots the ratio of measured shear strength, V_{test} to shear strength V_n calculated from Equations 4 through 6 without k factor versus the measured displacement ductility. Following the trend suggested in Figure 18, the factor k is defined to be equal to 1.0 for displacement ductility less than 2, and 0.7 for displacement ductility exceeding 6. For displacement ductilities between 2 and 6, the factor k varies linearly.

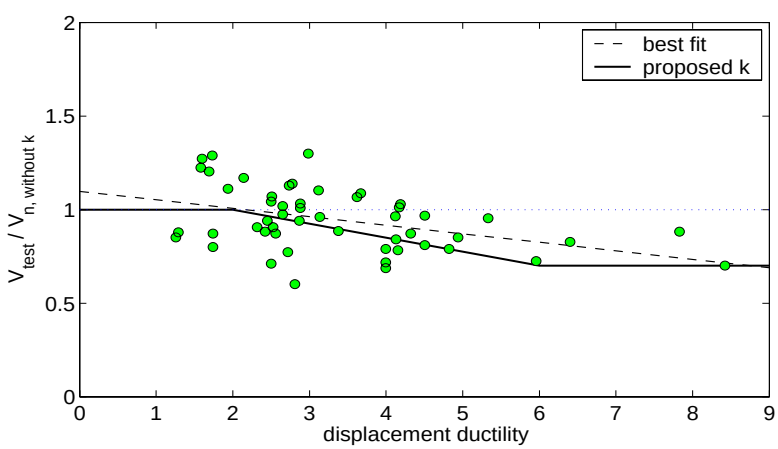

Figure 18 Relation between factor *k* and displacement ductility

Figure 19 plots the ratio of measured shear strength, V_{test} to shear strength V_n calculated from Equation 4 versus displacement ductility. The correlation between the measured and predicted shear strengths across the range of displacement ductility is reasonably well. The mean ratio of measured to calculated shear strength is 1.05 with a coefficient of variation of 0.15. Given the relatively low ductility associated with shear failure of columns like those considered in this study, the strength used in design or assessment normally will correspond to a lower-bound estimate of the shear strength. FEMA 356 [1] defines this as the lower five percentile of strengths expected. By this definition, and assuming a lognormal distribution in the strength ratio, the design strength should be taken as 0.80 times the nominal strength for the proposed model.

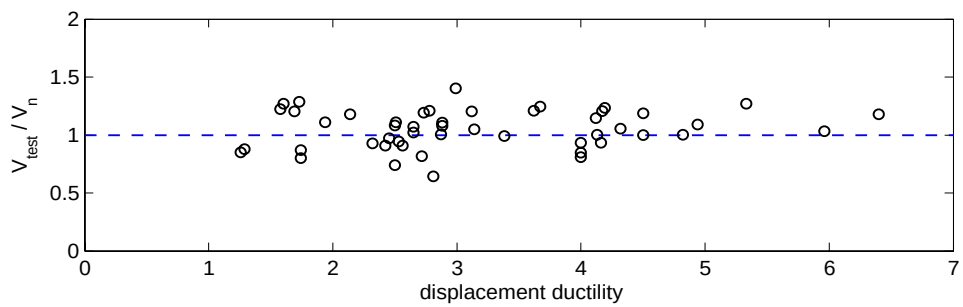

Figure 19 Ratios of measured to calculated shear strengths

CONCLUSIONS

Analytical and experimental findings from a research program investigating shear and axial failure of lightly reinforced columns are presented. All test columns experienced shear failure, though with different modes depending on the axial and lateral loading history. The lateral displacement components due to flexure, longitudinal bar slip, and shear were obtained. It was found that the contribution of bar slip deformations to total lateral displacement can be significant. Similarly, shear deformations can be considerably large after the development of large diagonal cracks. Monotonic flexural deformations calculated from fiber section moment-curvature analysis compared reasonably well with the experimental results. A monotonic bond-slip model is developed to characterize the bar slip deformation behavior. The calculated monotonic lateral load-slip displacement relations compared well with the measured cyclic response. A shear strength model is proposed including the contributions of transverse reinforcement and concrete. The effect of shear strength degradation is included in the transverse reinforcement and concrete contributions equally through a factor related to displacement ductility demand.

ACKNOWLEDGMENTS

This work was supported by the Pacific Earthquake Engineering Research (PEER) Center through the Earthquake Engineering Research Centers Program of the National Science Foundation under Award number EEC-9701568. The experiments were carried out in the research laboratories of PEER at the University of California, Berkeley.

REFERENCES

1. FEMA 356. November 2000. Prestandard and commentary for the seismic rehabilitation of buildings. Federal Emergency Management Agency. Washington D.C.
2. Lynn A. C., Moehle J. P., Mahin S. A., and Holmes W. T. 1996. Seismic evaluation of existing reinforced concrete building columns. *Earthquake Spectra*. Vol. 12, No.4, Nov. 1996. pp. 715-739

3. Sezen H. 2002. Seismic behavior and modeling of reinforced concrete building columns. *Ph.D. Thesis*. Department of Civil and Environmental Engineering. University of California, Berkeley.
4. XTRACT, Cross Sectional Analysis of Components, V6.2.0. Imbsen Software Systems. 2003. http://www.imbsen.com/xtract.htm
5. Mander J. B., Priestley M. J. N., and Park R. 1988. Theoretical stress-strain model for confined concrete," *Journal of Structural Engineering, ASCE*, V. 114, No.8, Aug. 1988. pp. 1804-1826.
6. Roy H. E. H., and Sozen M. A. 1964. Ductility of concrete. Proceedings of the *International Symposium on Flexural Mechanics of Reinforced Concrete*, ASCE-ACI, Miami, November 1964. pp. 213-224.
7. Lehman D. E., and Moehle J. P. 2000. Seismic performance of well-confined concrete bridge columns. PEER-1998/01. Pacific Earthquake Engineering Research Center, University of California, Berkeley. 316 pp.
8. Sezen H., and Moehle J. P. 2004. Shear strength model for lightly reinforced concrete columns. *Journal of Structural Engineering, ASCE* (in print)
9. Aschheim A. M., and Moehle J. P. 1992. Shear strength and deformability of RC bridge columns subjected to inelastic displacements. Technical Report: UCB/EERC 92/04. University of California, Berkeley. 93 pp.
10. Priestley M. J. N., Verma R., and Xiao Y. 1994. Seismic shear strength of reinforced concrete columns. *Journal of Structural Engineering, ASCE*, Vol. 120, No.8, Aug 1994, pp. 2311-2329
11. Konwinski C. M., Ramirez J. A., Sozen M. A. 1995. Shear strength of reinforced concrete columns subject to seismic loading. Proceedings of the National Seismic Conference on Bridges and Highways: Progress in Research and Practice, San Diego, California. December 10-13, 1995.